From *Advances in Coating and Drying of Thin Films*, F. Durst & H. Raszillier, Eds., Shaker Verlag, Aachen, 1999.

Theoretical and Numerical Modeling of Coating Flow on Simple and Complex Substrates including Rheology, Drying and Marangoni Effects

L. W. Schwartz
Coating Research Group
Department of Mechanical Engineering
University of Delaware
Newark, DE 19716 USA

Summary

We discuss the development of a comprehensive mathematical and numerical model for thin-layer flow of complex liquids on solid surfaces. The model includes physical and surface chemistry effects and allows direct prediction of the flow as it evolves in time, until the liquid has solidified. We pay particular attention to the substrate shape and wetting properties as well as viscosity dependence on flow stress and mixture composition. Important application areas are (i) decorative and protective coatings, and (ii) material processing. A particular research objective is the increased understanding of flow behavior that will aid in the design of new products and processes. Modeling results are shown for a number of problems, with experimental comparison, when available.

Introduction

Many fluid mechanics problems in the industrial and natural worlds involve flow of thin viscous films with a free surface. We will be concerned principally with a subclass of these where surface tension is important. Mathematical models will be given here for flows on flat and curved surfaces including other physical effects in several cases. These include gravity, compositional changes, substrate energetics and shear-thinning rheology. A major application area is the flow behavior of paints and other protective and decorative surface coatings. The prediction of liquid film behavior is also important in chemical and nuclear reactor design, agrochemical applications, as well as several biofluid applications including thin films on the cornea and in the lungs. Additional issues associated with surfactants are treated in a contributed paper at this meeting.

The mathematical models given here employ the long-wave or "lubrication" approximation. To leading order in the free-surface inclination, only a one-dimensional, unidirectional flow problem needs to be solved. Integrating across the thin dimension results in a reduction of the dimensionality of the problem. Many physical effects of

interest can then be modeled much more simply. Asymptotic derivations of lubrication theory, for two-dimensional problems with a free surface but without surface tension, are given by Benney[1] and by Atherton & Homsy[2] where surface tension is included. Lubrication theory has long been accepted as an appropriate model for thin layer flows and has been extensively investigated. Particularly noteworthy are the numerous contributions of L. E. Scriven at Minnesota and S. H. Davis at Northwestern and their many students.

In the following section we outline the procedure for obtaining the thin-layer approximation, starting from the equations of slow viscous flow with a free boundary. Wetting behavior of liquids on solid surfaces is discussed in section 2. The following section considers the modeling of flow on nonplanar surfaces while section 4 gives a simple model for drying. Modeling of temperature-gradient-driven flow, often termed Marangoni flow is briefly discussed followed by a section on Non-Newtonian effects.

1. Theory of Thin-layer Flows

Our primary interest is the flow of liquids in thin layers on a solid body (the 'substrate'). Because of the thinness of the liquid layer, a suitably defined Reynolds number will usually be small and the relevant problem is one of creeping motion with a moving free surface. The problem consists of the Stokes momentum equation

$$\nabla p = \mu \nabla^2 \mathbf{V} \tag{1.1}$$

and the incompressible continuity equation

$$\nabla \cdot \mathbf{V} = 0 \tag{1.2}$$

within the liquid region. The no-slip condition on an assumed stationary substrate is

$$\mathbf{V} = \mathbf{0} \; . \tag{1.3}$$

With $\mathbf{\Pi}$, and $\mathbf{n}$ signifying the stress tensor and a normal unit vector, respectively, conditions on the free surface are

$$\mathbf{\Pi} \cdot \mathbf{n} \cdot \mathbf{n} = \sigma \kappa, \tag{1.4}$$

and

$$\mathbf{\Pi} \cdot \mathbf{n} - \mathbf{n} \sigma \kappa = \nabla_s \sigma \; . \tag{1.5}$$

The kinematic boundary condition is

$$\mathbf{n} \cdot (\mathbf{V} - \dot{\mathbf{x}}) = 0 \; . \tag{1.6}$$

Here $\dot{\mathbf{x}}$ is the surface velocity, while p , μ , σ, and κ represent pressure, viscosity, surface tension and surface mean curvature, respectively. In the above we have allowed for tractions resulting from nonuniform surface tension. Such surface tension gradient effects can arise from a variety of causes including presence of surfactants, temperature differences, or compositional changes in a multi-component liquid. [If any of these effects are present, additional physical laws will be needed to complete the mathematical model.] $\nabla_s = (\mathbf{I} - \mathbf{nn})\nabla$ is the surface gradient operator.

The lubrication approximation is fundamentally a small slope theory. It is most easily obtained by separately scaling distances normal to the substrate as opposed to distances along the substrate. If the substrate is assumed to be planar, we can use cartesian coordinates. Let (x, y) be substrate coordinates and let z be distance measured normal to the substrate. Let h_0 be a characteristic coating thickness, while L is a distance along the substrate that needs to be traversed for the coating thickness to change by a factor that is $O(1)$. Then if $\epsilon = h_0/L$ is a small number, the n-th derivative representing change along the substrate has a magnitude that is $O(\epsilon^n)$. An immediate consequence of this scaling is, to leading order in ϵ, that the nonhydrostatic component of the pressure p is constant across the thin liquid layer; thus $p = p(x, y, t)$ only.

For thin cells where the liquid region is bounded by fixed or moving rigid walls, the small slope approximation leads to the well known Reynolds equation of lubrication theory; there the relevant problem to be solved is a Poisson-type equation for the pressure field. A special case of this, for parallel rigid bounding walls, is Hele-Shaw flow where the pressure plays the role of a velocity potential.[3]

For the free surface problems considered here, it is generally true that surface tension is an important effect. With the small slope approximation, the pressure in the liquid layer lying on a planar substrate, relative to the air above, will include a surface tension contribution

$$p^{(\sigma)} = -\sigma \nabla^2 h \tag{1.7}$$

using the two-dimensional Laplacian for the layer thickness h. Most often, in the applications considered here, gravity will also be important; the specific form of the gravity contribution to p depends on the orientation of each substrate element. The term $p^{(\sigma)}$ is nominally second-order small; in order to retain it, it needs to be 'specifically promoted,' i. e. we assume that its magnitude is comparable to any other driving term. Thus, if gravity is also considered, we state that typical substrate

scale lengths are of order

$$L_c = \sqrt{\frac{\sigma}{\rho g}} \ ,$$

the so-called capillary length. Therefore, practically speaking, we are more concerned with flow on centimeter-scale objects rather than meter-scale objects in terrestrial gravity. Of course it does no harm to retain the term in larger scale problems; in those cases surface tension effects can be expected to be restricted to thin boundary layers in regions of high surface curvature. Of course if gravitational acceleration is very small, as in space shuttle experiments for example, capillary effects become important at large physical dimensions.

We scale the governing equations and perform a systematic expansion in ϵ. The resulting leading-order evolution equation for surface motion, including surface tension and surface tension gradient terms, is

$$h_t = -\nabla \cdot \mathbf{Q} = \frac{1}{3\mu}\nabla \cdot (h^3 \nabla p) - \frac{1}{2\mu}\nabla \cdot (h^2 \nabla \sigma) \tag{1.8}$$

for flow on a planar substrate. The pressure is given by (1.7) and we have returned to dimensional quantities to more clearly indicate the origin of each term. The first equality in (1.8) represents integral mass conservation for a non-evaporating liquid coating, where the vector flux $\mathbf{Q}$ is

$$\mathbf{Q} = \int_0^h (u, v)\ dz \tag{1.9}$$

and (u, v) are velocity components in the directions (x, y).

We use finite difference methods for the solution of evolution equations such as (1.8) where p is given by (1.7). The simplest case, i.e. a layer whose thickness varies only in one space dimension with the surface tension held constant, still displays important issues. Because of the relation between pressure and curvature, this model equation is fourth-order in space. It is a diffusion equation, and like the simpler second-order heat equation, has a severe limitation on the maximum time step that can be used in an explicit finite-difference marching method, i.e.

$$\Delta t < C(\Delta x)^4$$

if h is uniformly of order one where C is a constant and Δx is the spatial step size. This limitation can be overcome by treating the equation implicitly; that is we evaluate the discrete approximation to the derivative at the new time level and solve a

banded system of equations for the increments in the vector $h_i(x_i,t) = h(i\Delta x,t)$. The simplest procedure is to evaluate the nonlinear prefactor h^3 at the old time level, resulting in a linear banded algebraic system for Δh_i. This is much more efficient computationally than treating this factor implicitly; in any event, the resulting first-order-accurate time integration can easily be checked for convergence under refinement. Discretization algorithms for one-dimensional and axisymmetric unsteady flows are given by Moriarty & Schwartz.[4,5] The two-dimensional version of (1.8) uses an alternating-direction implicit algorithm based on the scheme of Peaceman & Rachford[6] generalized to the present higher-order diffusive system.

1.1 A preliminary example

Consider a horizontal substrate that is wetted with a uniform thin layer of Newtonian liquid on its underside. This is a situation of unstable equilibrium; any small perturbation to uniformity will ultimately lead to the formation of a pattern of drops. Under the lubrication assumption, the governing equation is

$$h_t = -\sigma/(3\mu)\nabla\cdot[h^3\nabla\nabla^2 h] - \rho g/(3\mu)\nabla\cdot[h^3\nabla h]. \tag{1.10}$$

Using $L_c = (\sigma/\rho g)^{1/2}$ as the unit of length and $3\mu L^4/(\sigma h_0^3)$ as the unit of time, where h_0 is the initial layer thickness, reduces (1.10) to the dimensionless problem

$$h_t = -\nabla\cdot[h^3\nabla\nabla^2 h] - \nabla\cdot[h^3\nabla h]. \tag{1.11}$$

All parameters have been removed by the scaling. At the boundaries of the computational domain we impose the reflection symmetry conditions

$$h_n = h_{nnn} = 0.$$

The signs in (1.11) are such that the gravity term is destabilizing and the surface tension term provides stability.

An interesting feature of the simulation is the tendency for the drops to arrange themselves into a hexagonal pattern. This happens at late times in the simulation, via a sequence of small readjustments of drop positions. It is necessary for the computational domain to be large enough to include many drops for this pattern-forming tendency to be seen. A typical result is shown in Fig. 1. Experiments of Fermigier *et al*[7] also show this effect. Because the readjustments occur in the late-time nonlinear regime, no simple explanation for pattern forming has yet been offered.

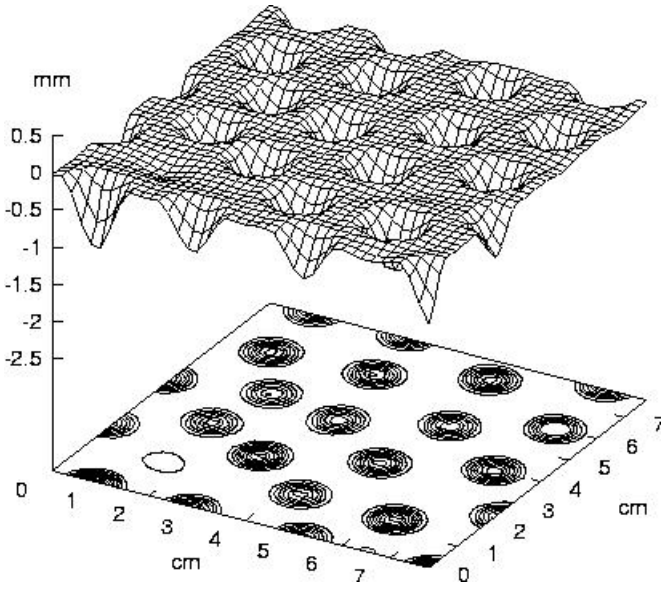

Figure 1: Simulation of droplet formation on the underside of a horizontal plate, exhibiting the tendency to form a hexagonal pattern. The initial state was a slightly-perturbed uniform layer.[8]

2. Finite-contact-angle Effects, Wetting and De-wetting, and Substrate Heterogeneity

Motion of liquids onto or from dry substrate areas require special treatment. Such contact-line motions contradict the usual no-slip boundary condition and a degree of "slip" must be introduced. Often the dry areas are due to lack of perfect wetting, as reflected in finite values of measurable contact angle. Both the required slip and the ability to prescribe an equilibrium contact angle are enabled by using a "disjoining" pressure term in the evolution equation. The pressure in the liquid is now given by

$$p = -\sigma\kappa - \Pi \approx -\sigma\nabla^2 h - \Pi \tag{2.1}$$

within the samll-surface-slope approximation. A two-term disjoining pressure is consistent with the Frumkin-Derjaguin model that relates static contact angles to measurable interfacial energies[9,10] and also can be used in dynamical cases:[11–13]

$$\Pi = B\left[\left(\frac{h^*}{h}\right)^n - \left(\frac{h^*}{h}\right)^m\right] . \tag{2.2}$$

B and the exponents n and m are positive constants with $n > m > 1$. The local

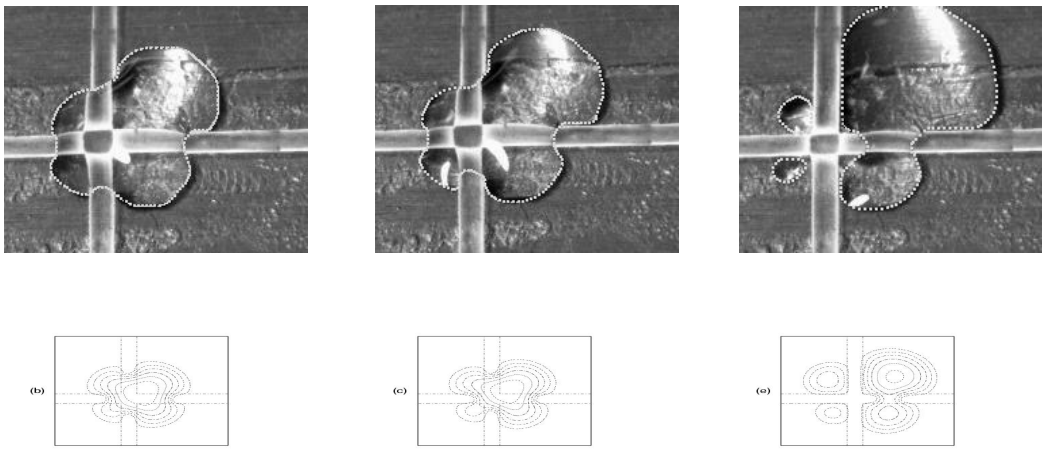

Figure 2: Experiment where a glycerin droplet is placed initially near the center of a cross of high-contact-angle material (top) and the corresponding theoretical calculation (bottom). From Schwartz & Eley[12].

disjoining energy density

$$e^{(d)}(h) = -\int_{h_*}^{h} \Pi(h')dh' \tag{2.3}$$

has a single stable energy minimum at a prescribed value h^*. For nominally-dry substrates, h^* plays the role of a slip coefficient, as required to overcome the moving-contact-line force singularity. The quantity B may be related to the equilibrium contact angle θ_e using

$$\sigma \cos\theta_e = \sigma - e^{(d)}(\infty) \tag{2.4}$$

which is the disjoining-model equivalent of the Young equation. $\theta_e(x, y)$ can be a prescribed "wettability" pattern on the substrate. In such cases B in Eqn. (2.2) is also a function of position. When Π is appended to the free surface evolution equation (1.8), a variety of problems on partially covered substrates can be treated. The exponent pair (n, m) controls the shape of the disjoining energy "well" at $h = h^*$.

The model equations are solved numerically. The model can be calibrated by comparison with several experiments. For complete wetting ($\theta_e = 0$), Tanner's[14] measurements of power-law spreading rates for an axisymmetric droplet are reproduced using realistically small values of h^*. Droplet spreading simulations at finite contact angle on a homogeneous substrate ($\theta_e = constant > 0$) show agreement with the experimental observations of Zosel.[15]

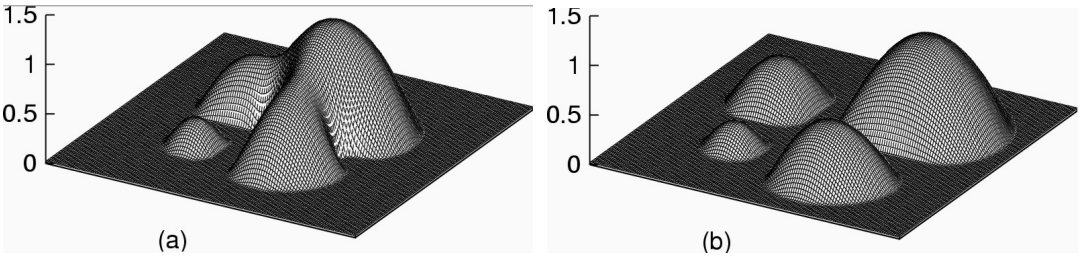

Figure 3: Two frames from a time-dependent simulation where, initially, a drop is placed near the center of a cross of poor-wetting material. (a) The time t is 0.35 in dimensionless units. (b) t = 0.70. Wire-cage views.[12]

We have performed a laboratory experiment (Fig. 2) to compare with drop spreading simulations.[12] A 26 μl drop of glycerin was placed near the center of a cross of 1 mm Teflon tape that had been fixed to a horizontal glass slide. Wetting forces cause the drop to break up into unequal fragments. Simulation results show detailed agreement with the experiment. However time-scale corrections need to be applied because (i) the simulation precursor layer h^* is overly large due to computational limitations, and (ii) the contact angles in the experiment are beyond the range of quantitative validity of the small-slope lubrication approximation. In both the experiment and the simulation, the motion proceeds in a "jerky" manner that is characteristic of capillary driven motions on nonuniform substrates. Two "wire-cage" pictures of the breaking drop in the simulation are shown in Fig. 3.

2.1 Simulation of contact angle hysteresis[13]

Simulations have been performed to investigate the origin of "contact angle hysteresis," an effect associated with the dissipation of energy when a liquid moves on mixed-wettable substrates. Periodic square patch patterns of "grease," i. e. high-contact-angle material, are used. We consider the motion of a drop, both in spontaneous motion, driven only by wetting forces, and also in a periodic forced motion. In spontaneous motion, the droplet edge can "hang up," either permanently or for long times, on the grease spots, as shown in Fig. 4. Quantitative measures of contact angle hysteresis (CAH) can be extracted from the numerical results and related to the defect pattern. CAH is a gross measure of the degree of imperfection of the substrate and is a characteristic of all real materials. Fig. 5 shows a hysteresis loop for forced periodic motion of a drop on a square pattern of grease patches as would be produced by injection/withdrawal cycles through a hypodermic needle for example.

A global energy balance equation may be written for this system

$$\dot{E}^{(\mu)} = -(\dot{E}^{(\sigma)} + \dot{E}^{(d)}) + \dot{W} \tag{2.5}$$

where the terms represent, respectively, the rate of viscous dissipation, the rates of change of capillary and disjoining energy, and the rate of working by injection forces (if present), each integrated over the substrate area. Injection and removal of liquid from a drop, and measurement of the pressure, as the volume is varied, can be used to probe the dynamic effect of particular substrate wettability patterns. In that case the total viscous work done is the time integral of $\dot{W}$, i. e. $\oint p\ dV$ where V is drop volume, $dV = w_i\ dA$ and the special integral sign denotes a full cycle. $w_i(x, y, t)$ is the imposed injection velocity distribution.

The area within the pressure-volume loop in Fig. 5 is the total energy dissipated per cycle. Shown for comparison, in the figure, is the hysteresis loop for same motion, but on a substrate of constant contact angle. The area is greater for the heterogeneous case, indicating the degree of extra damping, or energy extraction, that can be expected when the grease patches are used.

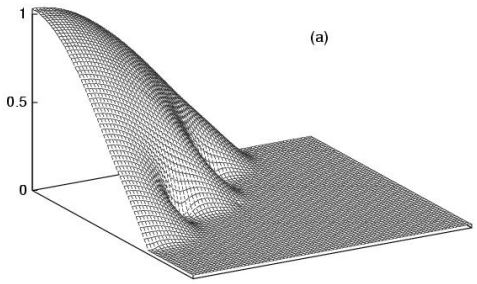

Figure 4: Simulation results for motions on heterogeneous substrates. The edges of a droplet de-wet on "grease" patches applied to the substrate.[13]

2.2 De-wetting

Dewetting is a ubiquitous phenomenon that is easily observed and often undesirable. Certain chemical and nuclear reactors employ wet walls for thermal protection when hot gases are contained under pressure. Dry spots on the walls can lead to catastrophic puncturing. Similarly, dewetting of the tear film in the eye is a potentially serious medical condition. In printing applications, the failure of a nominally uniform coating into a pattern of dewetted spots is called *reticulation*. Dewetting is sometimes intentional; waxy coatings on leaves of certain plants help them to channel dew and rainwater. The "balling up" of water on a freshly polished automobile indicates a high level of rust protection.

We can readily simulate spontaneous dewetting. Either a small localized pertur-

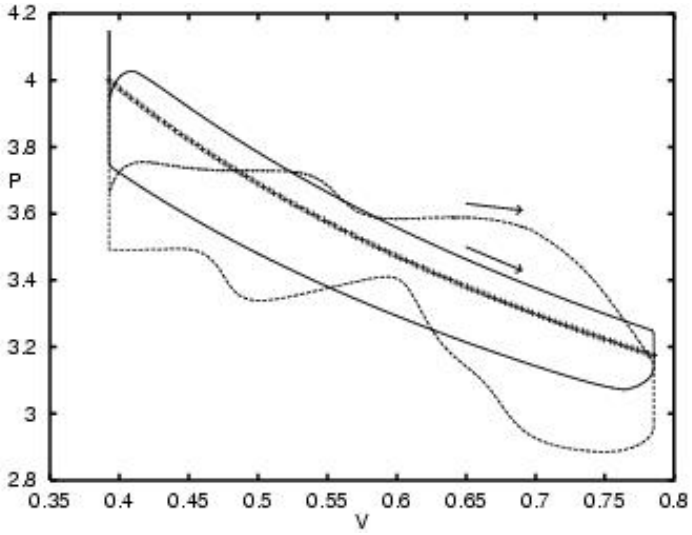

Figure 5: Pressure versus volume hysteresis loop for a periodic motion on a square pattern of grease patches.[13] The dissipated energy (area of loop) is greater for the heterogeneous substrate than for the uniform substrate case that is shown for comparison.

bation or random noise will initiate the dewetting process. We can apply a linear stability analysis to the evolution equation formed by combining equations (1.8) and (2.1 - 4). An initially uniform layer of thickness $h_0 >> h^*$ can be shown to have a most unstable wavelength proportional to $h_0^{(m+1)/2}$. The corresponding initial disturbance growth rate, proportional to $\sigma\theta_e^4/(\mu h_0^{2m-1})$ is a strong function of equilibrium contact angle θ_e. Two frames from a simulation of dewetting are shown in Fig. 6. The frames first show break-up into long ridges. These ridges then break up into drops. This two-stage process is also observed in other nonlinear pattern-formation processes.[16]

2.3 Nonuniform Substrates; a Microchip Application

A recent paper by Gau *et al*[17] presented experimental results for the deposition of cooled water vapor onto prepared mixed-wettable substrates. The substrate pattern consisted of alternating stripes of high and low contact angle material. Stripe widths were of the order of tens of microns. They observed, for a pattern of straight parallel strips, formation of continuous liquid channels of deposited water on the hydrophilic strips. The contact angle, at the wettability boundaries, increased as the quantity of deposited water increased, ultimately to values exceeding 90^o. At this point an instability developed, leading to bulges that overflowed onto adjacent hydrophobic regions.

They also observed that when the hydrophilic channels had corners, significant

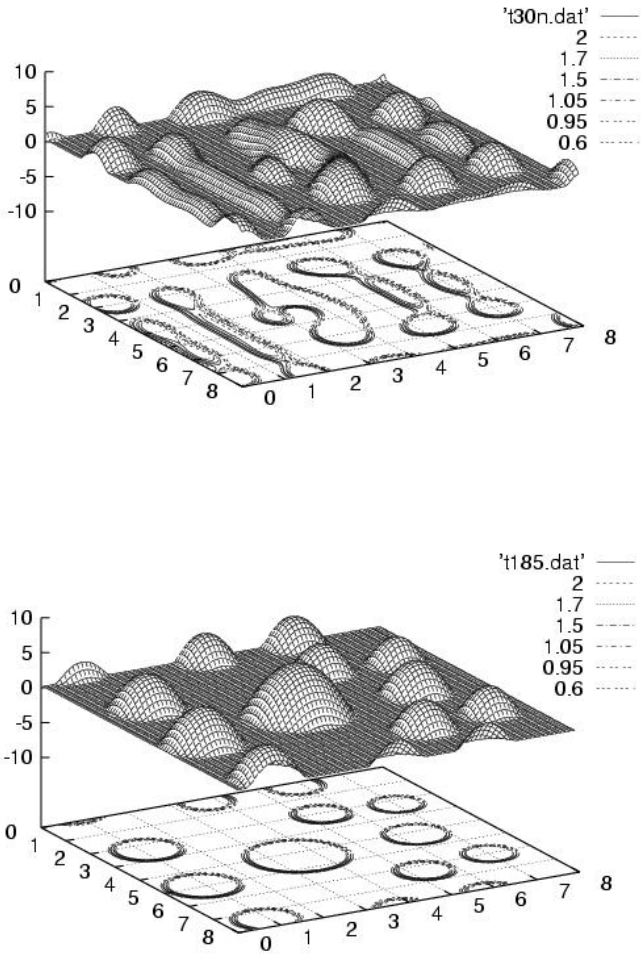

Figure 6: Simulation results showing spontaneous dewetting. An initially uniform liquid layer was perturbed with small noise. Plots of the free surface at later times first show formation of long ridges (top) which then break to form isolated droplets (bottom).

"puddling" occurred earlier there. The puddling increased with the amount of deposition, leading ultimately to bridging from one strip to the next. As they indicate, vapor deposition methods on patterned substrates is a technique that is applicable to microelectronics fabrication. In this context, the continuous channels are circuit elements and the deposited liquid metal, when solidified, will form a conductor. Thus the bridging is detrimental, representing a "short circuit." New generations of micro devices require circuits of even smaller dimensions; thus understanding the criteria for successful circuit fabrication, and the potential pitfalls, is of practical importance.

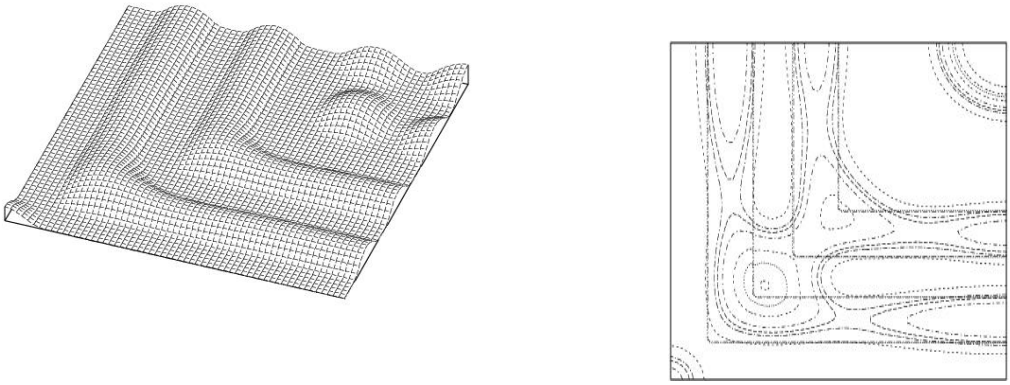

Figure 7: Modeling result for vapor deposition on a mixed-wettable substrate, as used to produce a microelectric circuit. Left: The liquid forms continuous conducting channels and isolated droplets, as seen in the experiments of Gau *et al*[17]. Right: Contour plot of modeling result at a later time, after more liquid has been deposited. The liquid overflows near the corner, bridging the gap between the two L-shaped regions and causing a short circuit.

In preliminary calculations we have reproduced the qualitative features observed in the experiment. Contact angle patterns in the calculation are prescribed on the substrate using the disjoining pressure function (2.2). Liquid is deposited uniformly at a constant rate as time proceeds in the simulation. The hydrophobic-hydrophilic contact angle ratio θ_2/θ_1 is an input variable. For large values of this ratio, there is no tendency to produce overflow puddles at corners. For smaller values of the ratio, the continuous liquid channels deform and overflow. Depending on the value of θ_2/θ_1, there is a maximum permissible total deposition before short-circuiting occurs. The left half of Fig. 7 is a wire-cage drawing of the simulation output showing two right-angle low-contact angle channels and the developed liquid ridges. Some overflow is apparent near the inside corners. There are also isolated droplets produced as the liquid balls up on hydrophobic regions. Each of these features is quite apparent in the microphotograph of the experiment (Fig. 5 of Ref. 17). Once the maximum permissible volume has been exceeded, a liquid bridge is formed in the neighborhood of the corners, as seen in the contour plot on the right of the figure.

3. Treatment of Nonplanar Substrates

The theory of thin-layer coating flows may be extended to include flow on substrates that are not flat. Several different procedures may be formulated, depending on the type of problem considered.

3.1 Substrates of constant mean curvature

For flow on cylindrical or spherical objects, for example, it is possible to refor-

mulate the thin-layer equations using a coordinate system that fits the surface. An example of a calculation performed in cylindrical polar coordinates is shown in Fig. 8. The evolution of initially uniform layers on solid horizontal rods of various radii has be found. The liquid is assumed to be non-evaporating and Newtonian. Ultimately a pattern of pendant drops is formed on the lower side. Derivation of the thin layer equations and details of the numerical solution procedure are given in Ref. 18.

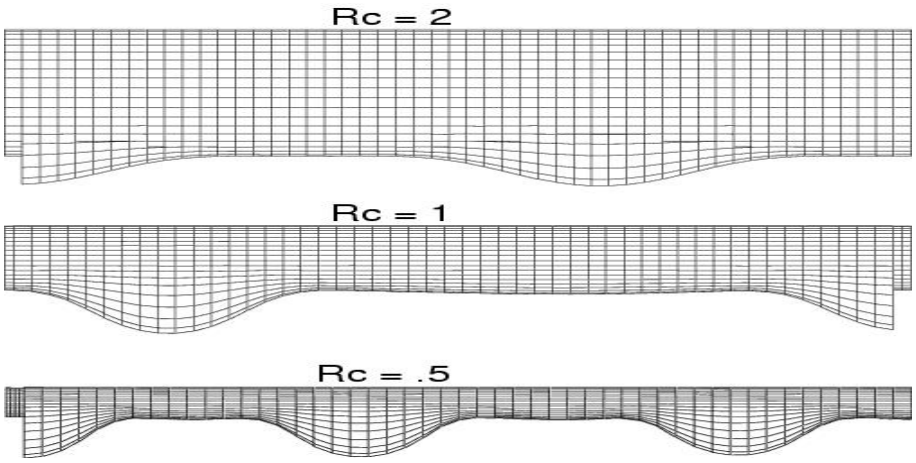

Figure 8: Calculated droplet shapes hanging from horizontal cylindrical rods. Results are given for three values of rod radius, measured in units of the capillary length L_c.[18]

3.2 Corner defects

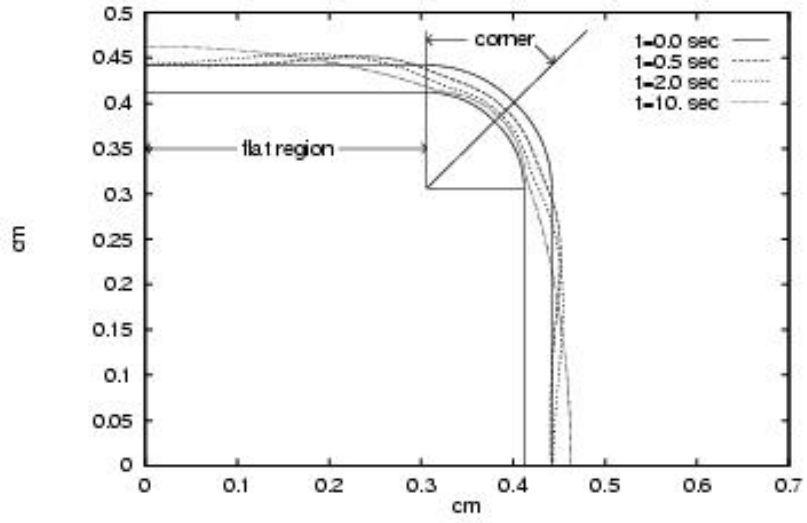

Figure 9: Reference case for flow away from an outside corner for a non-evaporating Newtonian liquid of constant surface tension. Here the corner radius is 0.1 cm. The coating profiles are shown at various times. Note that the thickness of the coating layer has been magnified for clarity.[19]

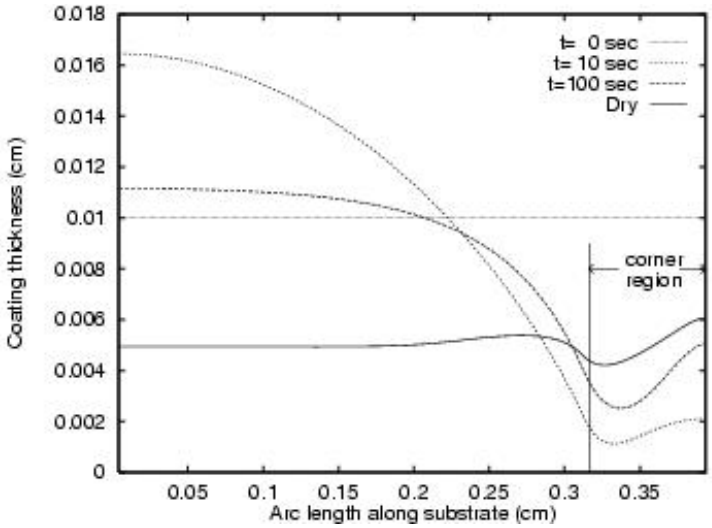

Figure 10: Coating thickness versus position and time for the substrate shown in Fig. 9 (“Un-wrapped”). Here drying is considered and the drying rate is optimized so as to use Marangoni forces to “pull back” the coating after the initial displacement by capillary forces.[20]

Sometimes objects to be coated have cross-sections composed of straight seg-

ments and curved arcs. In this case, an approximate theory can be formulated using an equivalent flat substrate, where the dominant effect of the curved segments is to produce an effective capillary "overpressure" distribution that is determined by the curvature variation. Lubrication-type equations using this approach are capable of modeling the development of *corner defects*, such as the flow away from outside corners and puddling at inside corners.[19,20] Fig. 9 shows the flow history for an initally uniform coating that is applied to a substrate of square cross-section with rounded corners of small radius, a wrought iron fence post for example. Surface tension causes rapid flow away from the corner. Final dry coating thicknesses may be expected to be small there. Indeed, failure of coatings at fence post edges is commonly observed.

It is possible, at least in principle, to mitigate this problem if a coating that developed Marangoni forces as it dries is used, as discussed in the next section. If the drying rate is selected appropriately, a virtually-uniform final dry coating can be achieved, as shown in Fig. 10.

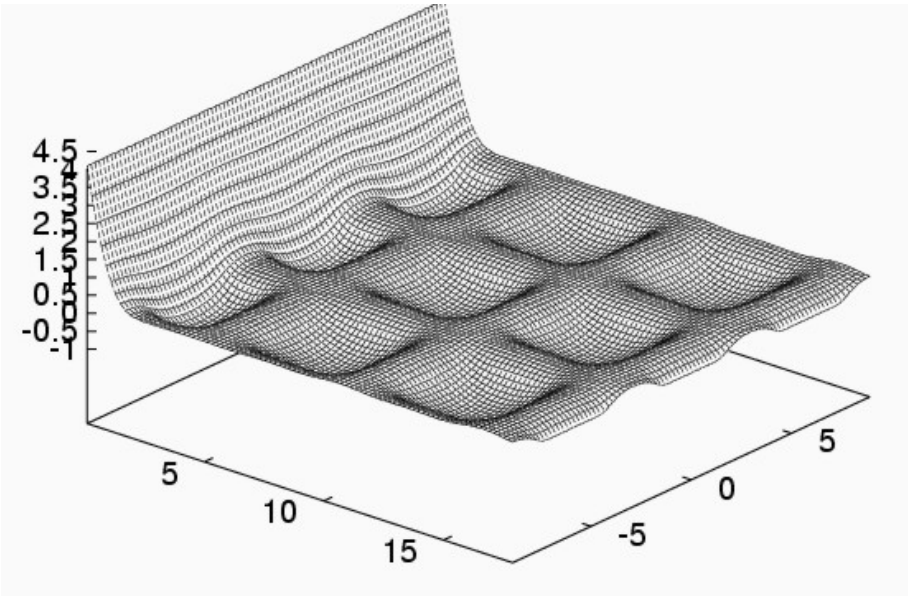

Figure 11: A frame in a time-dependent calculation of the withdrawal of liquid from gravure cells. The liquid meniscus is "pinned" at the left boundary and the gravured substrate (not shown) is moving to the right.[23]

3.3 Behavior of liquid on a pattern of gravure cells

Physical roughness, such as the gravure cells that are often used in rotary coating, can be expected to act in a similar fashion to chemical heterogeneity when a liquid meniscus moves on a substrate. It is possible to include a roughened substrate

in the lubrication formulation. It may be shown that the evolution equation need only be modified by inclusion of the substrate shape function in the "permeability," i. e. the factor of proportionality between the liquid flux and the pressure gradient[21]. It is often convenient to allow the substrate to move with time while the computational window is fixed to the oscillating liquid free surface. A model problem is an extension of the well-known Landau-Levich[22] problem for the withdrawal of a moving plate from a bath of liquid. We consider the plate to have a periodic pattern of roughness or "cells." The plate moves with constant speed U to the right while the liquid meniscus is pinned at the left end of the computational window. As seen in Fig. 11, the downward pressure of the meniscus acts so as to "scrape" liquid from the cells. Because of surface tension, a certain residual fraction remains in each cell, determined primarily by the cell size and cell shape. Further details, including applications in the coating and printing industry, are given in Schwartz *et al*.[23]

4. Effects of Compositional Changes and Drying

Certain binary liquid mixtures have surface tension values that vary with the fractional composition. A commonplace example is an alkyd paint whose surface tension increases as the solvent evaporates. Strong surface tension gradient effects can arise for a thin, nonuniform coating layer of the mixture. Often, there is surprising behavior; an initial hump in the coating may turn into a local depression in the final dry coating. Our extended model can reproduce such phenomena. Representative equations[24], are

$$\frac{\partial h}{\partial t} = -\nabla \cdot \left[\frac{h^2}{2\mu} \nabla\sigma + \frac{h^3}{3\mu} \nabla^2 h \nabla\sigma + \frac{h^3}{3\mu} \sigma \nabla\nabla^2 h - \frac{h^3}{3\mu} \rho g \nabla h \right] - E \qquad (4.1)$$

and

$$\frac{\partial (ch)}{\partial t} = \nabla \cdot (Dh\nabla c - c\mathbf{Q}) \qquad (4.2)$$

These two partial differential equations are solved simultaneous for the layer thickness h and the "resin fraction" c. Additional relations are supplied that relate the viscosity μ, the diffusivity D, the surface tension σ and the evaporation rate E of the solvent fraction. This simple drying model postulates a known relation between evaporation rate and local mixture composition. Admittedly, this is an oversimplification of the relevant thermodynamics.

Figure 12 shows two frames from the simulation of drying with developed surface-tension-gradient effect. Initial humps in the coating are seen to become depressions in the final dry coating.

The anomalous rebound effect for a drying alkyd paint was measured experimen-

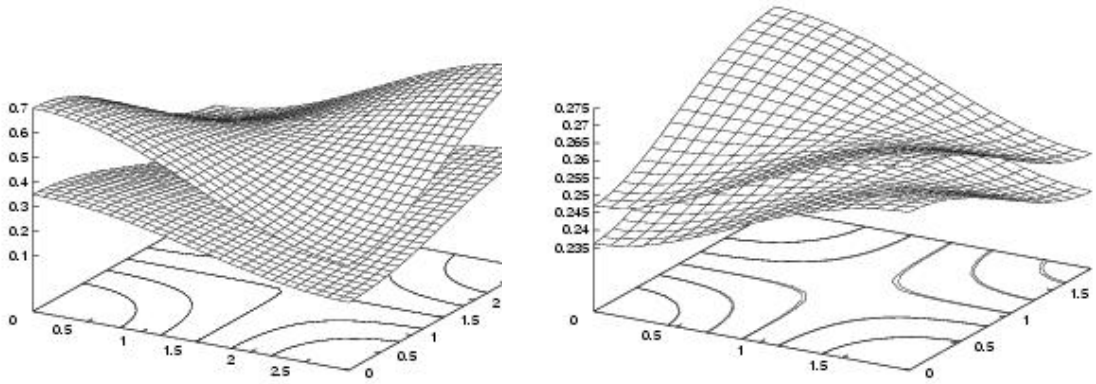

Figure 12: Leveling of an uneven coating with compositional changes; The coating height and "resin height" are shown. Left: Initial state; Right: The coating is almost dry. Maragoni effect causes initial humps to dry as depressions.

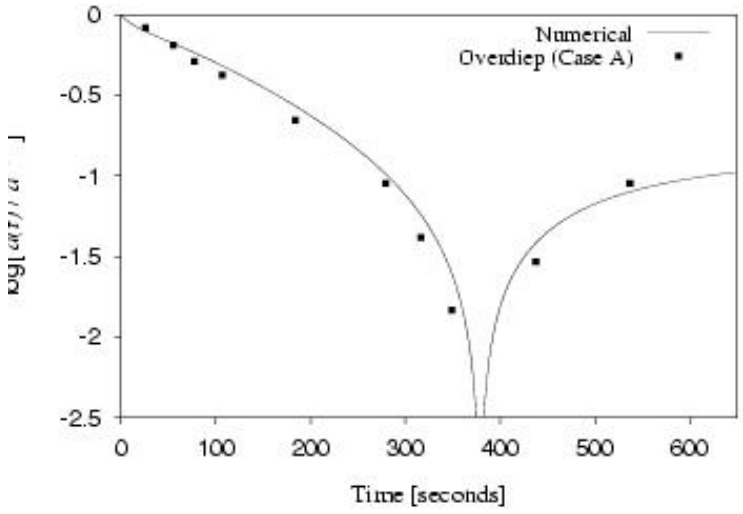

Figure 13: Comparison of experiments[25] and model prediction[24] for the amplitude of a initial bump in a drying layer of alkyd paint. Surface tension gradient effects, that develop as the mixture dries, cause the ampltude to first fall and then rise.

tally by Overdiep.[25] Comparison of the numerical prediction for the height of an initial hump with experimental measurements is shown in Fig 13. The simulation used experimentally measured parameter values and functional dependencies taken from the literature.

5. Marangoni Flows Driven by Temperature Gradients

Because surface tension generally decreases with increasing temperature, liquid motion can be driven by an imposed temperature gradient $\partial T/\partial x$. If this gradient is assumed constant, a driving term of the form $1/(2\mu)\ \tau\ \partial(h^2)/\partial x$, where $\tau = (\partial\sigma/\partial T)(\partial T/\partial x)$, may be appended to the evolution equation of section (1.1). The resulting driven flow, analogous to one produced by wind shear, is known to be unstable and develops growing "fingers." Figure 11 shows a comparison of experimental results[26] with our simulation[27] at a particular instant of time.

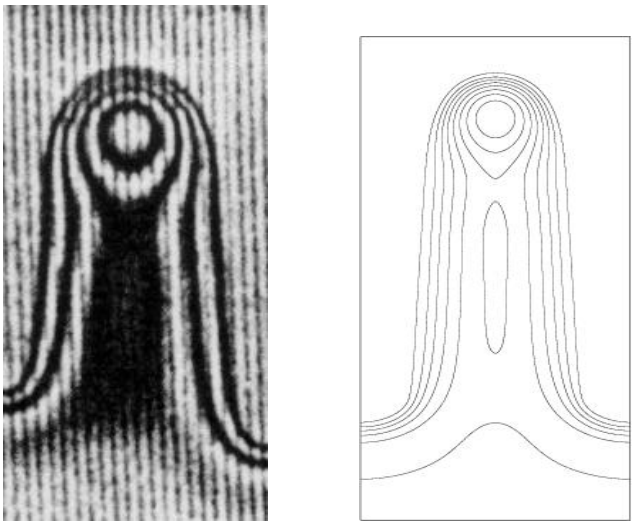

Figure 14: Left: Interferograph from the experiment of Cazabat[26] for thin-film "fingering" driven by a temperature gradient (reproduced with permission of Elsevier Pubs.). Right: Corresponding simulation result.[27]

This problem is closely related to fingering in draining flow on a vertical wall.[28] Simulation results have also been compared with published linear stability analyses for the two problems.[29,30] In each, the most unstable wavenumber and initial growth rates in the simulation are close to the predictions of the linear analyses.

6. Non-Newtonian Rheology

The equations can be extended to account for non-Newtonian flow behavior. There are many different models that propose relationships among the viscosity, stress, and strain rate. A particularly attractive choice is the Ellis model which describes a liquid that, at low levels of stress, flows at constant viscosity, while at high stress levels displays power-law shear-thinning behavior.

As a preliminary example we show that the Ellis Model can relieve the moving-contact-line singularity when a liquid moves onto a dry substrate. In contrast to

previous models that allow contact line motion, it is no longer necessary to abandon the no-slip condition at the substrate in the vicinity of the contact point. While the stress is still unbounded at the contact point, the integrated stress or contact-line force is finite. A three–constant Ellis viscosity model is employed which allows a low-shear Newtonian viscosity and may thus be used to model essentially Newtonian flows where shear-thinning only becomes important in the immediate vicinity of the contact point. The calculation finds the steady progression of a uniform coating layer down a vertical substrate.[31]

We consider the motion of a semi–infinite uniform coating layer draining down a previously dry, vertical substrate where x is measured downward along the wall, y is the normal coordinate, and $h(x)$ is the steady free-surface shape to be determined. The origin of coordinates is at $x = 0$ and the liquid-gas interface meets the wall at this point with an included angle θ_c. The wall is moving upward at a speed U selected so as to render the motion steady. Far upstream of the contact point, the uniform liquid thickness is h_1.

For downward flow in a vertical wall, the shear stress in the liquid is

$$\tau = (\sigma h_{xxx} + \rho g)(h - y). \tag{6.1}$$

The liquid is assumed to obey an Ellis constitutive law[32]

$$\tau = \eta u_y,$$

where

$$\frac{1}{\eta} = \frac{1}{\eta_0}\left(1 + \left|\frac{\tau}{\tau_{1/2}}\right|^{\alpha-1}\right). \tag{6.2}$$

Here η is the viscosity, η_0 the viscosity at zero shear stress, $\tau_{1/2}$ the shear stress at which the viscosity is reduced by a factor of 1/2, and α is a power–law index. When $\alpha = 1$, the liquid is Newtonian, while for $\alpha > 1$, the liquid is shear thinning. The Ellis viscosity model incorporates power–law behavior at high shear stresses while allowing for a Newtonian plateau at low shear stresses. Because the free surface of the coating is stress free, and the shear stress in the liquid far away from the contact point is quite small, this is a particularly appropriate rheological model.

A speed U is selected so as to make the free surface steady in the moving coordinate system. In dimensionless variables, the ordinary differential equation satisfied by the liquid surface is

$$(\hat{h}_{\hat{x}\hat{x}\hat{x}} + 1)\hat{h}^3\left[1 + \frac{3}{\alpha+2}\left|(\hat{h}_{\hat{x}\hat{x}\hat{x}} + 1)B\hat{h}\right|^{\alpha-1}\right] = \hat{h}\left[1 + \frac{3}{\alpha+2}B^{\alpha-1}\right], \tag{6.3}$$

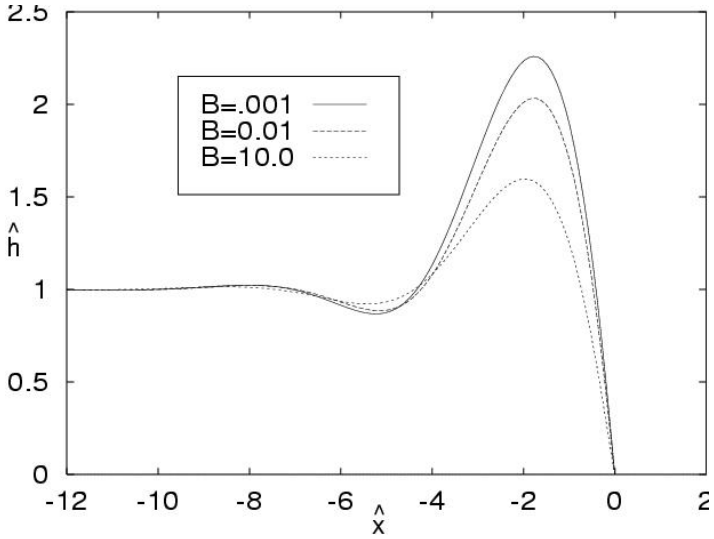

Figure 15: Coating flow of an Ellis fluid liquid on a vertical wall.[31] The total force at the contact line is finite because of shear-thinning effect. Curves show coating profiles for several values of the stress ratio B in Eqn. (6.3).

where $\hat{h} = h/h_1$, $\hat{x} = [\rho g/((\sigma h_1)]^{1/3} x$, and $B = \rho g h_1/\tau_{1/2}$.

Equation (6.3) can be solved by a shooting method, starting at a large distance upstream of the contact point where $\hat{h} \to 1 \ \text{ as } \ x \to -\infty$. The additional boundary conditions on $\hat{h}_{\hat{x}}$ and $\hat{h}_{\hat{x}\hat{x}}$ are derived from a linearized form of (6.3), appropriate to the far upstream region where the surface oscillation amplitude is very small. Specific details are given in Ref. 31 where the procedure of Tuck & Schwartz[33] is generalized to the present Ellis model liquids. For a given set of upstream boundary conditions, the free surface profile equation is integrated numerically all the way to the contact point using a fourth-order Runge-Kutta scheme. The slope, where the free surface meets the substrate, and the maximum 'overshoot' of the liquid layer, are found as part of solution; they are, in general, functions of both the stress ratio B and the shear-thinning exponent α. Profiles for $\alpha = 2$ and various values of B are shown in Figure 15. It may be verified that, while the wall shear stress becomes unbounded at the contact point, the total force is integrable provided $\alpha > 1$. Weidner & Schwartz[31] also suggest reasons why nominally Newtonian liquids may shear thin at high levels of stress. Adiabatic viscous heating is known to cause a reduction in viscosity, for example. There is experimental evidence for such viscosity reduction at very high stresses for Newtonian liquids.

The introduction of somewhat more complex rheology into the multi- dimensional lubrication model can be accomplished without difficulty and constitutes a useful generalization, even when contact-line motion is not an issue. We consider, as an example, sagging resulting from "overspray," when coating a vertical panel. "Sagging" refers here to the pattern of "fingers" or drip marks that often are observed

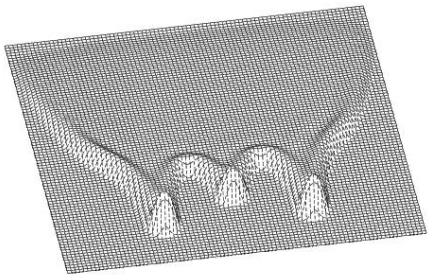

Figure 16: Sagging pattern for a Newtonian coating showing pronounced drip marks.

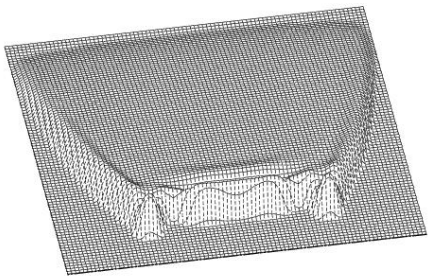

Figure 17: Sagging pattern for a shear-thinning coating. Drip marks are much less developed.

when coating vertical surfaces. Once the coating has dried, sagging patterns typically form an unsightly defect; thus a basic understanding of the mechanisms leading to drip marks will have important implications for the design of new coatings in order to minimize this effect. It is clear that surface tension contributes to defect formation. It is also known that the effect is less pronounced when the rheology is shear-thinning, as compared to a Newtonian coating.

As the initial condition for the simulation, we consider a uniform thin coating on the vertical substrate. In addition there is a “hyper-ellipsoidal” mound with the

equation

$$h(x,y) = h_0[1 - A(x - x_0)^4 - B(y - y_0)^4]^{1/4} \tag{6.4}$$

superimposed on the uniform layer. A, B, x_0 and y_0 are constants specifying the major and minor axes of the mound and its center, respectively. The hyperellipsoid represents a thick overspray, perhaps applied inadvertently in practice. The simulation assumes a surface tension of 30 dynes/cm and we take the thin coating layer to have a wet thickness of 0.02 cm while the maximum height of the overspray mound is 0.4 cm. The parameters A and B are selected to make the width of the mound equal to 7.2 cm while the width, in the downward direction, is 1.4 cm. The time scale is proportional to the viscosity μ; for $\rho g = 10^3$ gm/cm^2/sec^2, and a Newtonian viscosity of 3 poise, the characteristic time is $T^* \approx 1$ sec.

Figure 16 shows the fate of the initial overspray mound after 107 seconds have elapsed for the Newtonian coating. The figure shows developed drip marks and large capillary ridges at the troughs. By contrast, Figure 17 is a simulation for a shear-thinning Ellis liquid, with exponent $\alpha = 2$ in the rheological equation (6.2). The liquid has advanced down the wall about the same distance, however the drip marks are much less well developed.

Acknowledgment

This work is supported by the ICI Strategic Research Fund, The State of Delaware, and the NASA Microgravity Program.

References

1. Benney, D. J., "Long waves on liquid films," *J. Math. & Phys.* **45**, 150 (1966).
2. Atherton, R. W. & Homsy, G. M., "On the derivation of evolution equations for interfacial waves," *Chem. Eng. Comm.* **2**, 57 (1976).
3. Sherman, F. S., *Viscous Flow*, 1990, McGraw-Hill, New York.
4. Moriarty, J. A. & Schwartz, L. W., "Effective slip in numerical calculations of moving-contact-line problems," *J. Engineering Math.* **26** 81 -86, 1992.
5.Moriarty, J. A. and Schwartz, L. W., "Dynamic considerations in the closing and opening of holes in thin liquid films," *J. Coll. and Interf. Sci.*,**161**, 335-342, 1993.
6. Peaceman, D. W. & Rachford, H. H., "The numerical solution of parabolic and elliptic differential equations," *SIAM J.* **3**, 28 (1955).
7. Fermigier, M., Limat, L., Wesfreid, J. E., Boudinet, P. & Quilliet, C., "Two-dimensional patterns in Rayleigh-Taylor instability of a thin layer," *J. Fluid Mech.***236**, 349-383, 1992.
8. Schwartz, L. W., "Unsteady simulation of viscous thin-layer flows", *Free-Surface*

Flows with Viscosity pp. 203 - 233, 1998, Ed. P. A. Tyvand, Computational Mechanics Publ., Southampton.
9. Frumkin, A. N., "On the phenomena of wetting and sticking of bubbles," *Zhur. Fiz. Khim.* **12**, 337 (1938) [In Russian].
10. Deryaguin, B. V., "Theory of the capillary condensation and other capillary phenomena taking into account the disjoining effect of long-chain molecular liquid films," *Zhur. Fiz. Khim.* **14**, 137 (1940) [In Russian].
11. Mitlin, V. S. & Petviashvili, N. V., "Nonlinear dynamics of dewetting: kinetically stable structures," *Phys. Lett. A* **192**, 323 - 326, 1994.
12. Schwartz, L. W. & Eley, R. R., "Simulation of Droplet Motion on Low-Energy and Heterogeneous Surfaces," *J. Colloid Interface Sci.* **202**, 173 - 188, 1998..
13. Schwartz, L. W., "Hysteretic effects in droplet motions on heterogeneous substrates," *Langmuir* **14**, 3440-3453, 1998.
14. Tanner, L., "The spreading of silicone oil drops on horizontal surfaces," *J. Phys. (D)* **12**, 1473 - 1484, (1979).
15. Zosel, A., "Studies of the wetting kinetics of liquid drops on solid surfaces," *Colloid & Polymer Sci.* **271**, 680 (1993).
16. Manneville, P., *Dissipative structures and weak turbulence*, 1990, Academic Press, Boston.
17. Gau, H., Herminghaus, S., Lenz, P. & Lipowsky, R., "Liquid morphologies on structured surfaces; from microchannels to microchips," *Nature* **283**, 46 - 48, 1999.
18. Weidner, D. E., Schwartz, L. W. & Eres, M. H., "Simulation of coating layer evolution and drop formation on horizontal cylinders," *J. Colloid Interface Sci.* **187**, 243 - 258, 1997.
19. Schwartz, L. W. & Weidner, D. E., "Modeling of coating flows on curved surfaces," *J. Engineering Math.* **29**, 91 - 103, 1995.
20. Weidner, D. E., Schwartz, L. W. & Eley, R. R., "Role of surface tension gradients in correcting coating defects in corners," *J. Colloid Interface Sci.* **179**, 66 - 75, 1996.
21. Kim, J. S. and Kim, S. and Ma, F., *J. Appl. Phys.*, **73**, 422 - 428, 1993.
22.Levich, V. G., *Physiochemical Hydrodynamics*, 1962, Prentice-Hall, Englewood Cliffs.
23. Schwartz, L. W., P. Moussalli, P. Campbell, & R. R. Eley "Numerical modeling of liquid withdrawal from gravure cavities in coating operations," *Trans. Inst. Chem. Engrs.* **76**, 22-29 (1998).
24. Eres, M. H., Weidner, D. E. & Schwartz. L. W. "Three-dimensional direct numerical simulation of surface-tension-gradient effects on the leveling of an evaporating multi-component fluid," *Langmuir* **15**, 1859-1871, 1999.
25. Overdiep, W. "The levelling of paints," *Progress in Organic Coatings*, **14**, 159 - 175, 1986.
26. Cazabat, A. M, Heslot, F., Carles, P. & Troian, S. M., "Hydrodynamic fingering

instability of driven wetting films," *Adv. Colloid Interf. Sci.* **39**, 61 - 75, 1992.
27. Eres, M. H., Schwartz. L. W., & Roy, R. V. "Fingering Instabilities of Driven Thin Coating Films," *Phys. of Fluids* 1999 (submitted).
28. Schwartz, L. W., "Viscous flows down an inclined plane: Instability and finger formation," *Phys. of Fluids* **A1**, 443 - 445, 1989.
29. Kataoka, D. E. & Troian, S. M., "A theoretical study of instabilities at the advancing front of thermally driven coating films" *J. Colloid Interf. Sci.* **192**, 350 -362, 1997.
30. Spaid, M. A. & Homsy, G. M., "Stability of Newtonian and viscoelastic dynamic contact lines," *Phys. Fluids* **8**, 460 -478, 1996.
31. Weidner, D. E. & Schwartz, L. W., "Contact-line motion of shear-thinning liquids," *Phys. Fluids* **6**, 3535 - 3538, 1994.
32. Byrd, R. B., Armstrong, R. C. & Hassager, O., *Dynamics of Polymeric Liquids v. 1*, 1977, Wiley, New York.
33. Tuck, E. O. & Schwartz, L. W., "A numerical and asymptotic study of some third-order ordinary differential equations relevant to draining and coating flows," *SIAM Review* **32**, 453 - 469, 1990.